HYDROLOGICAL PROCESSES
Hydrol. Process. **22**, 4850–4869 (2008)
Published online 29 July 2008 in Wiley InterScience
(www.interscience.wiley.com) DOI: 10.1002/hyp.7104

Intercomparison of remote sensing-based models for estimation of evapotranspiration and accuracy assessment based on SWAT

Yanchun Gao[1]* and Di Long[1,2]

[1] *Institute of Geographic Sciences and Natural Resources Research, Chinese Academy of Sciences, P.O. Box 9719, Beijing 100101, China*
[2] *Graduate University of Chinese Academy of Sciences, Beijing 100039, China*

Abstract:

An intercomparison of daily actual evapotranspiration (ET) estimates from the single-source models (SEBAL and SEBS) and the two-source models (P-TSEB and S-TSEB) using remotely sensed data was performed to examine their utilities and limitations under a wide range of land covers and different meteorological conditions. The accuracy of ET estimates from remote sensing-based models of a selected watershed on 23 June 2005 (DOY 174) presenting large air drying power and marked contrast in underlying surface characteristics, and 25 July 2005, (DOY 206) in contrast to the meteorological and underlying surface conditions of DOY 174, were evaluated in terms of SWAT-based ET. The ET estimates from the two methodologies are shown to be comparable, indicating that S-TSEB has the highest accuracy with relative errors of 2·2% and 5·6% with reference to SWAT-based ET for DOY 174 and 206, respectively. Hence it was selected to be the basis for performing an intercomparison with other remote sensing-based models. Single-source models are very sensitive to KB^{-1} parameter, rendering marked differences in ET estimates because of different treatments of roughness length for heat transfer. SEBAL and SEBS yielded mean absolute percentage difference (MAPD) versus S-TSEB within 26·22% and 26·56% for DOY 174 and within 9·11% and 11·69% for DOY 206, respectively, indicating their applicability to higher vegetation cover and soil moisture availability areas under small air drying power condition. P-TSEB generated MAPD versus S-TSEB within 41·15% for DOY 174 and 8·79% for DOY 206, implying that P-TSEB is highly consistent with S-TSEB under small air drying power and less contrast in soil moisture conditions, whereas noticeable discrepancies occur under large air drying power and marked contrast in soil moisture circumstances, in particular for sparse cover. The performance of P-TSEB largely depends on the meteorological and underlying surface conditions, both exerting significant influences on the extent of coupling between vegetation and soil. Copyright © 2008 John Wiley & Sons, Ltd.

KEY WORDS evapotranspiration; single-source model; two-source model; SWAT; accuracy assessment; intercomparison

Received 9 October 2007; Accepted 23 May 2008

INTRODUCTION

Evapotranspiration (ET), including evaporation from soil surface and vegetation transpiration, is an important variable for water and energy balances on the Earth's surface. Much research and many applications regarding water resources, agriculture and forest management require a knowledge of ET over a range of spatial and temporal scales. Numerous theories and practices have proven that ET involves complex interactions between water and energy fluxes, and is controlled by the factors of water and energy availability and the mechanism of water–heat transfer, varying with terrain, surface characteristic and meteorological condition (Betts *et al*., 1997; Hipps and Kustas, 2000; Wegehenkel *et al*., 2005). The main methods (e.g. lysimeter, Bowen ratio, eddy correlation system) used conventionally to measure ET are subject to individual, field or landscape scales (Baldocchi *et al*., 2001; Brotzge and Kenneth, 2003; Yunusa *et al*., 2004; Gentine *et al*., 2007), but regional or continental ET cannot be measured directly or interpolated due to the inherent spatial heterogeneity of the land surface. Satellite provides an unprecedented spatial distribution of critical land surface variables, such as surface albedo, fractional vegetation cover, land surface temperature, so numerous physical and empirical remote sensing-based models in combination with ancillary surface and/or atmospheric data have been developed to estimate ET for clear sky days (Bastiaanssen *et al*., 1998a; Bastiaanssen, 2000; Jiang and Islam, 2001; Su, 2002; Wang *et al*., 2006), and the applicable range of soil-vegetation-atmosphere transfer (SVAT) schemes has been expanded owing to assimilating the directional radiometric surface temperature (Norman *et al*., 1995; Kustas and Norman, 1997).

Different models have different assumptions and complexity. For instance, the single-source models, such as the Surface Energy Balance Algorithm for Land (SEBAL) (Bastiaanssen *et al*., 1998a) and the Surface Energy Balance System (SEBS) (Su, 2002), regard vegetation and soil as one 'big leaf' with identical temperature and aerodynamic resistance for water–heat transfer at the same height. In contrast, the two-source models, in which vegetation and soil are independent sinks or sources of

* Correspondence to: Yanchun Gao, Institute of Geographic Sciences and Natural Resources Research, Chinese Academy of Sciences, P.O. Box 9719, Beijing 100101, China. E-mail: gaoyanc@igsnrr.ac.cn

heat fluxes, such as Series Two-Source Energy Balance (S-TSEB) (Shuttleworth and Wallace, 1985) used for modelling the component (vegetation and soil) exchange of heat and water with the atmosphere, and Parallel Two-Source Energy Balance (P-TSEB) (Kustas and Norman, 1999; Norman *et al*., 1995) assuming no heat flux exchanges between vegetation and soil, parameterize the component heat fluxes separately. Consequently, it is crucial for proper use of these models to extensively compare and contrast their performances over various land covers and under different meteorological conditions at regional scales, and to examine the utilities and limitations of their rationales.

It has been proven that the remote sensing-based models could generate reasonable ET distribution across a wide range of land covers due to assimilating remotely sensed land surface temperature, which could signal the variation in evaporative fraction (Jiang and Islam, 2001; Batra *et al*., 2006), a key element affecting the variation in actual ET. However, the heat flux and ET amount at pixel scale have been viewed with some skepticism despite validation performed with tower-based flux observations or more regionally with aircraft for several retrievals because: (1) the accuracy of land surface variables/parameters retrieved from remotely sensed data has not achieved a completely perfect level; (2) the remote sensing-based models are usually based on the energy balance equation. Although the relative amount or distribution of each component of the energy balance equation can be reasonable over the scene, the absolute amount of latent heat flux may not absolutely accord with reality. Therefore, accuracy assessment is a fundamental component for remote sensing-based models.

The use of a hydrological approach may be an alternative way to validate ET estimates from remote sensing-based models at watershed scales (Bastiaanssen *et al*., 1998b; Kite and Droogers, 2000). We consider that a representative watershed can be selected to carry out the validation experiment and the Soil and Water Assessment Tool (SWAT) (Arnold *et al*., 1998) can be employed to compute ET of the whole watershed for accuracy assessment. SWAT is a continuous time, physically and spatially semi-distributed model developed to simulate the impact of management decisions on water, sediment and agricultural chemical yields in river basins. The SWAT-based ET of the whole watershed could be used as the standard for accuracy assessment of remote sensing-based models based on the following reasoning:

(1) The hydrological model is capable of yielding an accurate ET amount for a watershed, but cannot provide high resolution ET distribution data like the remote sensing-based models. The remote sensing-based model is capable of generating reasonable ET distribution, but the ET amount at pixel scale is in doubt and needs to be evaluated;
(2) Although the ET resolution of remote sensing-based models at the pixel scale differs from that of SWAT at the hydrological response units (HRUs) or sub-basin scale, the ET amount from SWAT of the whole watershed can reflect a realistic ET after simulation of hydrological processes during a rational period accurately performed, because the fundamental elements of hydrological processes, such as precipitation, runoff, can be measured directly and therefore the ET amount can be restricted rationally to the water balance equation;
(3) If the ET estimate from a particular remote sensing-based model of the whole watershed is close to the SWAT output, the conclusion could be made that the remote sensing-based model not only generates a reasonable ET distribution estimate, but also yields reliable ET amounts at the pixel scale.

One of the critical problems in such a comparison is the difference in temporal scale between the remote sensing-based instantaneous latent heat flux and SWAT-based daily ET. Accordingly the remote sensing-based latent heat flux should be extended to daily scale ET for comparison with the hydrological approach.

The objectives of the study were (1) to compare the remote sensing-based daily ET extended from the instantaneous latent heat flux with SWAT-based daily ET to evaluate the accuracy of remote sensing-based models; (2) to make an intercomparison and contrast of daily ET from SEBAL, SEBS, P-TSEB, and S-TSEB under a series of land covers and meteorological conditions on the basis of the model having the highest accuracy in terms of SWAT, aiming at exploring the performance, applicability and error source of remote sensing-based models.

EXPERIMENTAL WATERSHED

The validation experiment was conducted in a watershed with an area of 1850 km^{-2} between 41°02′ to 41°37′N and 116°08′ to 116°45′E, located around Dage hydrological station in the upper Chao river, which lies in a transition zone between the Inner Mongolia Plateau and the North China Plain (Figure 1). Administratively it belongs to Fengning Manchu Autonomous County, Hebei Province. The north-west part of the watershed is along the southern border of the Inner Mongolia plateau, the south-east part lies along the northern foothills of Yanshan Mountains, and the outlet is in the south-east. Elevation decreases from north-west to south-east and ranges from 2213 m to 650 m above sea level, with a mean of 1164 m. The climate of the area is the transition zone from semi-humid to semi-arid continental monsoon climate in temperate zone. According to meteorological and hydrological records from 1950 to 2005, the mean annual air temperature of this area is approximately 6·8 °C (coldest −11·7 °C in January and warmest 22·4 °C in July). Its mean annual precipitation and mean annual runoff are 457·1 mm and 54·9 mm, respectively. In the watershed, cultivated land accounts for 26·8% of

DOI: 10.1002/hyp

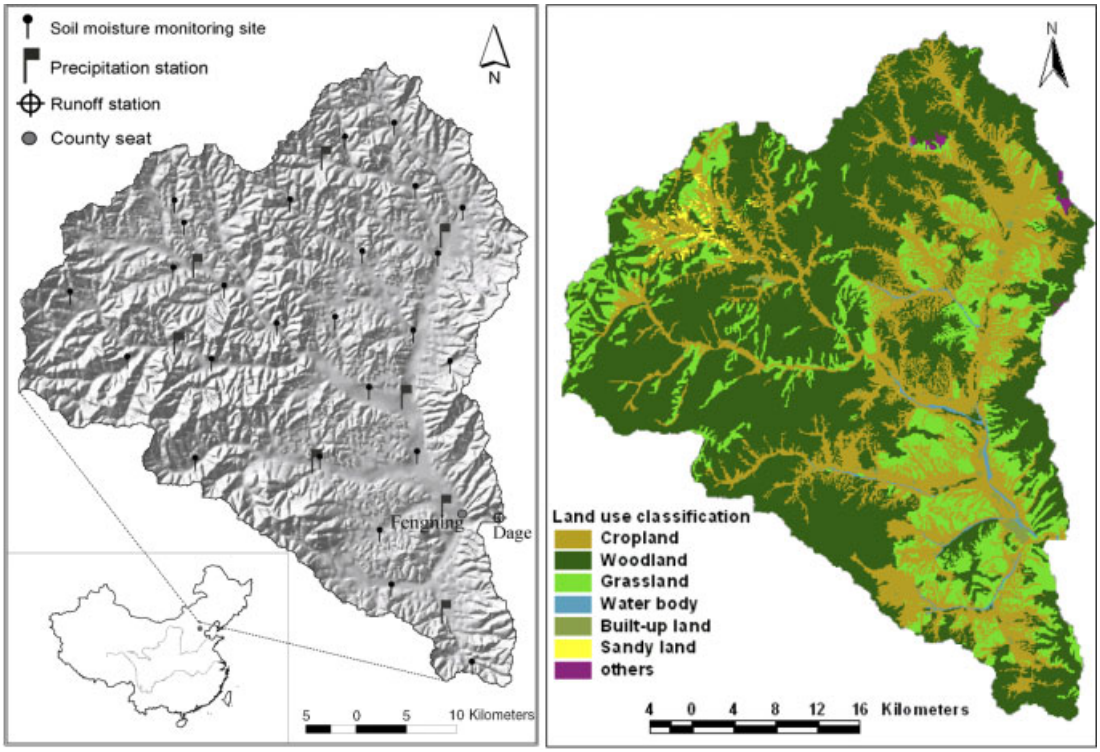

Figure 1. Location of the experimental watershed in China and its land use map

the area, forestland 54·7%, grassland 16·5%, water body 0·6%, built-up land 0·7%, sandy land 0·5%, and others 0·2%. It is the source of water into Miyun Reservoir, the main drinking water sources for Beijing. Being located in a mountainous area with little anthropogenic influence the precipitation–runoff transformation is mainly in the form of surface runoff and lateral flow, so that the groundwater change in the deep aquifer does not need to be considered by SWAT in the simulation of hydrological processes. There are eight meteorological stations and one runoff station in the watershed.

MODEL DESCRIPTION

Four remote sensing-based models were selected for this study including the single-source models SEBAL and SEBS, and the two-source models P-TSEB and S-TSEB. This section first describes the similarities and differences in these models, including the specific algorithms for certain variables/parameters employed in this study. And then elaborates the fundamental mechanism of SWAT with how to obtain its related variables/parameters.

Model similarities

The single-source and two-source modelling schemes are based on energy balance in the vertical direction above a horizontal surface, assuming advection and that the light energy required for photosynthesis is negligible. The evaporative process is, to a large extent, controlled by the soil resistance to evaporation and the bulk stomatal resistance to transpiration. To circumvent the problem related to the lack of information on these surface resistances, the latent heat flux from remote sensing-based models is usually calculated as the residual of the surface energy balance equation (Kustas *et al*., 1994; Moran *et al*., 1994; Boegh *et al*., 2002). Consequently, the energy balance equation can be expressed as:

$$\lambda E = R_n - G_{soil} - H \tag{1}$$

where λ is the latent heat of vaporization (J kg^{-1}), E is the evapotranspiration rate (kg m^{-2} s^{-1}), R_n the net radiation flux density (W m^{-2}), G_{soil} the soil heat flux density (W m^{-2}), and H the sensible heat flux density (W m^{-2}).

The instantaneous net radiation is determined by surface characteristics, atmosphere properties, solar zenith angle, etc.

$$\begin{aligned} R_n &= (1-r)S_{in} + (L_{in} - L_{out}) - (1-\varepsilon)L_{in} \\ &= (1-r)S_{in} + \varepsilon_a \varepsilon \sigma T_a^4 - \varepsilon \sigma T_{sur}^4 \end{aligned} \tag{2}$$

where S_{in} is the incoming short wave radiation (W m^{-2}), L_{in} is the incoming long wave radiation (W m^{-2}), L_{out} is the outgoing long wave radiation (W m^{-2}), r is the surface albedo, which can be retrieved from Band 1, 2, 3, 4, 5, and 7 of Landsat5 TM (Chen and Ohring, 1984; Koepke *et al*., 1985; Bastiaanssen *et al*., 1998a; Bastiaanssen, 2000; Wang *et al*., 2000), ε is the surface emissivity, which can be estimated by the Normal Difference Vegetation Index (NDVI) retrieved from the red and near infrared bands using semi-empirical relationships (Van de Griend and Owe, 1993; Bastiaanssen *et al*., 1998a), T_{sur} is the surface temperature (K), which can be retrieved by the thermal infrared band, Band

DOI: 10.1002/hyp

6 of Landsat5 TM (Bastiaanssen, 2000; Chander and Markham, 2003). The atmospheric emissivity ε_a can be estimated from atmospheric temperature and humidity (Brutsaert, 1975), σ is the Stefan–Boltzman constant ($5{\cdot}67 \times 10^{-8}$ W m^{-2} K^{-4}). The slope and azimuth of tilted land can be extracted from digital elevation model (DEM) for calculation of the solar incidence of the incoming short wave radiation (Tasumi *et al.*, 2000). The instantaneous net radiation therefore can be parameterized using a combination of the above parameters/variables and other auxiliary data, such as satellite overpass time and Julian day number (Bastiaanssen *et al.*, 1998a; Su, 2002). The soil heat flux is considered to be a fraction of the net radiation (Kustas *et al.*, 1994; Moran *et al.*, 1994; Bastiaanssen *et al.*, 1998a; Campbell and Norman, 1998). In this study, the soil heat fluxes from all models were estimated using the algorithm developed by Bastiaanssen *et al.* (1998a) except that from SEBS using the algorithm by Su (2002).

The main difference between the single-source and the two-source models is the algorithm for sensible heat flux, namely how to deal with the heat fluxes of vegetation and soil, either the mixture as single-source models or the individual as two-source models. After calculating the sensible heat flux (discussed in the next section), the evaporation fraction can be obtained as follows:

$$\Lambda = \frac{\lambda E}{\lambda E + H} = \frac{R_n - G_{soil} - H}{R_n - G_{soil}} \tag{3}$$

where Λ is the evaporation fraction. From several observational studies, the evaporation faction has been found to be fairly time invariant during the daytime (Shuttleworth *et al.*, 1989; Nichols and Cuenca, 1993; Brutsaert and Chen, 1996; Crago and Brutsaert, 1996). And thus the daily actual ET can be estimated from multiplying the evaporation fraction by the daily net radiation as follows:

$$\mathrm{ET_a} = \frac{86400 \times \Lambda \times R_{day}}{\lambda} \tag{4}$$

where $\mathrm{ET_a}$ is the daily actual evapotranspiration (mm day^{-1}), R_{day} is the daily net radiation (W m^{-2}). The daily net radiation is also an important variable determining the ET amount according to Equation (4), but the observed daily net radiation at the meteorological station is representative of flat area (Zhang *et al.*, 2005; Allen, *et al.*, 2006). As the terrain of the watershed is complex with undulating topography, the impact of sloping surfaces on the available radiation should be considered pixel by pixel when calculating of the daily net radiation (Allen *et al.*, 2006).

Model differences

SEBAL and SEBS. SEBAL assumes that the temperature difference between surface and reference height is linearly proportional to the remotely sensed surface temperature T_{sur} and can be specified by using two extreme pixels, termed the coldest pixel and the warmest pixel. The coldest pixel is of the lowest surface temperature with higher fractional vegetation cover, based on the assumption that at the limiting case the sensible heat flux is zero, contrary to the warmest pixel with the highest surface temperature and no latent heat flux. In this study, the coldest pixel is of surface temperature 291·3 K and 288·0 K for DOY 174 and DOY 206, respectively, for forest with very high vegetation cover. And the warmest pixel is of surface temperature 314·7 K and 312·5 K for DOY 174 and DOY 206, respectively, for sandy land, with roughness length for momentum transfer of 0·01 m. The model corrects the friction velocity and aerodynamic resistance for unstable conditions on the basis of Monin-Obukhov similarity hypothesis using the iterative method (Bastiaanssen *et al.*, 1998a; Bastiaanssen, 2000; Kimura *et al.*, 2007).

The sensible heat flux therefore can be expressed as:

$$H = \rho c_p (aT_{sur} + b)/r_{ah} \tag{5}$$

$$r_{ah} = [\ln(\frac{z-d}{z_m}) - \psi_m][\ln(\frac{z-d}{z_h}) - \psi_h]/k^2 u \tag{6}$$

where a and b are linear regression coefficients that are site and scene specific, ρ is the air density (kg m^{-3}), c_p is the air specific heat at constant pressure (J kg^{-1} K^{-1}), r_{ah} is the aerodynamic resistance for heat transport(s m^{-1}), z is the reference height (m), d is the zero plane displacement (m), z_m is the roughness length for momentum transfer, z_h is the roughness length for heat transfer. The KB^{-1} parameter ($= \ln(z_m/z_h)$) of nominal value of 2·3 is applied, namely $z_h = z_m/10$. u is the velocity at the reference height (m s^{-1}), k is the von Karman constant, ψ_m and ψ_h are the stability correction factor for momentum and sensible heat, respectively.

The d, z_m were estimated by formulas as follow (Brutsaert, 1982):

$$d = 0{\cdot}667 h_c \tag{7}$$

$$z_m = 0{\cdot}123 h_c \tag{8}$$

where h_c is the vegetation height (m), which could be specified by establishing the empirical relationship between the vegetation index and h_c from field campaigns (Kimura *et al*, 2007).

In SEBS, an algorithm permits one to determine the roughness length for heat transfer. Thus the KB^{-1} parameter is distributed rather than a fixed value as in SEBAL.

$$kB^{-1} = \frac{kC_d}{4C_t \frac{u_*}{u(h)}(1 - e^{-n_{ec}/2})} f_c^2 + 2 f_c f_s \frac{k^{u_*}\Big/ u(h) \times z_m \Big/ h_c}{C_t^*} + kB_s^{-1} f_s^2 \tag{9}$$

$$kB_s^{-1} = 2{\cdot}46(R_{e^*})^{1/4} - \ln[7{\cdot}4] \tag{10}$$

$$n_{ec} = C_d \times \mathrm{LAI} \times u(h)^2 / 2u_*^2 \tag{11}$$

where f_c is the fractional canopy coverage and f_s is its complement, C_d is the drag coefficient of the foliage

DOI: 10.1002/hyp

elements, C_t is the heat transfer coefficient of the leaf, u_* is the friction velocity (m s^{-1}), $u(h)$ (m s^{-1}) is the horizontal wind speed at the canopy top. The heat transfer coefficient of the soil is given by $C_t^* = Pr^{-2/3}Re_*^{-1/2}$, P_r is the Prandtl number and the roughness Reynolds number $Re_* = h_s u_*/\upsilon$, h_s is the roughness height for soil (m). The kinematic viscosity of the air is $\upsilon = 1{\cdot}327 \times 10^{-5}(P_0/P)(T/T_0)^{1{\cdot}81}$ (m s^{-1}), with P and T the ambient pressure and temperature and $P_0 = 101{\cdot}3$ kPa, $T_0 = 273{\cdot}15$ K, n_{ec} is the within-canopy wind speed profile extinction coefficient, LAI is the leaf area index which can be estimated by NDVI.

A formulation was proposed to determine the evaporative fraction on the basis of the energy balance at limiting wet and dry cases. Detailed descriptions of these algorithms and parameters can be found in Su (2002) and Su *et al*. (2005).

P-TSEB and S-TSEB. The main difference between P-TSEB and S-TSEB is whether or not there is turbulent exchange between vegetation and soil, resulting in different complexities and applicabilities in calculation of the heat fluxes under certain vegetation structure and fractional vegetation cover. The resistance networks of P-TSEB and S-TSEB are illustrated in Figure 2.

For TSEB, the partitioning of component net radiation is based on the fractional vegetation cover and vegetation structure (Choudhury *et al*., 1994; Kustas and Norman, 1999). Thus the component energy balance equation can be expressed as:

$$R_{n,c} = H_c + \lambda E_c \tag{12}$$

$$R_{n,s} = H_s + \lambda E_s + G_{soil} \tag{13}$$

where S and C denote the soil and canopy, respectively.

For P-TSEB:

$$H_c = \rho c_p (T_c - T_a)/r_a \tag{14}$$

$$H_s = \rho c_p (T_s - T_a)/(r_a + r_s) \tag{15}$$

where r_a is the aerodynamic resistance from the canopy air layer above the soil to a reference height, r_s is the aerodynamic resistance to heat transfer from the soil. The parameterization of r_a and r_s can be found in Norman *et al*. (1995), Kustas and Norman (1999). In this study, the formulas of resistances in Kustas and Norman (1999) were adopted due to some amelioration and modification performed. T_a, T_c and T_s are air, canopy and soil temperature, respectively.

The fractional vegetation cover at a certain view angle θ was used to partition the satellite-based directional radiometric temperature (Becker and Li, 1990; Norman *et al*., 1995) as follows:

$$T_{rad}(\theta) = [f_c(\theta)T_c^4 + f_s(\theta)T_s^4]^{1/4} \tag{16}$$

where T_{rad} is the remotely sensed radiometric temperature, $f_c(\theta)$ is the fractional vegetation cover, $f_s(\theta)$ is $1 - f_c(\theta)$. In combination of Priestley–Taylor equation (Priestley and Taylor, 1972) and Equation (16), the component temperatures (T_s and T_c) and fluxes (H_s, λE_s and H_c, λE_c) could be partitioned without necessarily requiring multiangular remotely sensed data for solving Equation (16). More details about the procedures for partitioning component fluxes can be found in Norman *et al*. (1995).

For S-TSEB, first introduced by Shuttleworth and Wallace (1985), the component energy balance equations can be expressed as:

$$\begin{aligned} H &= H_c + H_s \Rightarrow \rho c_p (T_h - T_a)/r_a \\ &= \rho c_p (T_c - T_h)/r_{ac} + \rho c_p (T_s - T_h)/r_{as} \end{aligned} \tag{17}$$

$$\begin{aligned} \lambda E &= \lambda E_c + \lambda E_s \Rightarrow \rho c_p (e_h - e_a)/\gamma r_{aa} \\ &= \rho c_p (e^*(T_c) - e_h)/\gamma (r_{sc} + r_{ac}) \\ &\quad + \rho c_p (e^*(T_s) - e_h)/\gamma (r_{as} + r_{ss}) \end{aligned} \tag{18}$$

where h denotes the in-canopy source height, γ is the psychrometric constant, T_h is the temperature at in-canopy source height, $e^*(T)$ is the saturate vapour pressure at temperature T; e_a is the actual vapour pressure at reference height, e_h is the vapour pressure at in-canopy source height, r_{as} is the aerodynamic resistance between ground surface and within canopy source height (Shuttleworth and Gurney, 1990), r_{ac} is the bulk boundary layer resistance to heat and water vapour in the canopy (Choudhury and Monteith, 1988), r_{ss} is the soil resistance to evaporation, r_{sc} is the bulk stomatal resistance. Norman *et al*.

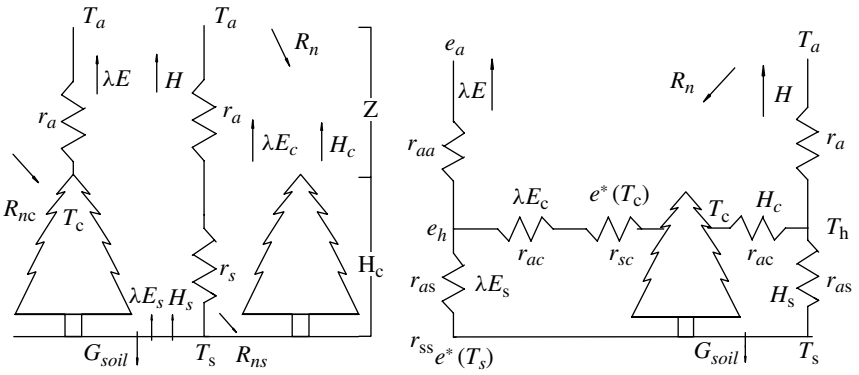

Figure 2. The schematic diagram of the energy fluxes of P-TSEB (left) and S-TSEB (right). S and C denote soil and canopy, respectively

DOI: 10.1002/hyp

(1995) has assimilated the directional radiometric temperature for solving Equation (17) and (18) as follows:

(a) The vegetation heat fluxes and its temperature on the basis of Priestly–Taylor equation are expressed as:

$$H_c = \rho c_p \frac{T_c - T_h}{r_{ac}}$$
$$= R_{n,c} - \lambda E_c = R_{n,c}(1 - 1{\cdot}26 f_g \frac{\Delta}{\Delta + \gamma}) \Rightarrow$$
$$T_c = [\frac{r_{ac}}{\rho c_p} R_{n,c}(1 - 1{\cdot}26 f_g \frac{\Delta}{\Delta + \gamma})] + T_h \quad (19)$$

where Δ is the slope of saturated vapour pressure; f_g is the fraction of the LAI that is green.

(b) Equation (16) is simplified as the linear area-weighted relationship:

$$T_{rad}(\theta) \cong f_c(\theta) T_c + f_s(\theta) T_s \quad (20)$$

(c) The temperature at in-canopy source height can be obtained by combining Equations (17), (18), and (20):

$$T_h = \frac{T_{rad} r_a + T_a f_s r_{as} + \frac{H_c}{\rho c_p}(f_s r_a r_{as} - f_c r_a r_{ac})}{f_s r_{as} + r_a} \quad (21)$$

(d) The energy balance equation for soil can be solved by inputting T_h from Equation (21) and T_c from Equation (19):

$$H_s = \rho C_p (\frac{T_s - T_h}{r_{as}}) \quad (22)$$
$$\lambda E_s = R_{n,s} - H_s - G \quad (23)$$

(e) If $\lambda E_s < 0$, the nonphysical solution is obtained, and then order $\lambda E_s = 0$ due to the nonexistence of daytime condensation at the soil surface, readjusting the energy balance for soil and T_h:

$$T_h = \frac{T_{rad} r_a + T_a f_c r_{ac} + \frac{H_s}{\rho c_p}(f_c r_a r_{ac} - f_s r_a r_{as})}{f_c r_{ac} + r_a} \quad (24)$$

(f) Using the readjusted T_h from Equation (24) to redetermine the total sensible heat fluxes from components and redistributing the vegetation heat fluxes in terms of Equation (17) and (12), thus the component heat fluxes can be obtained.

SWAT modeling scheme

The water balance is the driving force behind the movement of pesticides, sediments and nutrients in a watershed, so the hydrology simulation is the core mechanism of SWAT. It simulates the processes including precipitation, infiltration, surface runoff, evapotranspiration, lateral flow and percolation. Groundwater is simulated at two aquifer systems, a shallow unconfined aquifer contributing to the return flow and a deep confined aquifer, besides pumping in the watershed, disconnected from the system. In SWAT, the watershed is first partitioned into a number of sub-watersheds or sub-basins based on a threshold area, and secondly each sub-watershed is further divided into one or several homogeneous hydrological response units (HRUs) representing unique combinations of soil and land use similar enough to affect hydrology. The subdivision of the watershed enables the model to reflect difference in ET of various land covers and soil types. Runoff is predicted separately for each HRU and routed to obtain the total runoff for the watershed, which increases accuracy and gives a much better physical description of the water balance. The accuracy of ET amount of each sub-basin and their aggregated values for the whole watershed simulated by SWAT seems reliable because the semi-distributed model is based on the water balance that reflects the reality of hydrological processes, in which the ET amount is confined logically to the amount of primary hydrology elements. The precipitation and runoff can be readily obtained from hydrological stations. Other hydrological processes can be simulated by appropriately optimizing model parameters until the simulated runoff is accordant with the observed counterparts as accurately as possible. A complete description of SWAT model components (Version 2000) can be found in Arnold *et al*. (1998) and Neitsch *et al*. (2002).

A 30 m grid DEM was available for the discretization procedure. The flow gauging station, Dage, was imposed as the outlet of the whole watershed, and a threshold area of 3,000 ha (minimum area drained through a cell for the latter to be defined as a stream cell) was selected to discretize the watershed into 31 sub-basins. The land use map was available from the visible and near infrared bands of TM5 by supervised classification and the pedological map (1: 1,000,000) was available with its textural profile description for creating the soil database. The bulk density, saturated hydraulic conductivity, available water content (the difference between field capacity and wilting point) required for soil database to run SWAT were generated by the functions proposed by Saxton and Rawls (2006). The overlay of soil and land use maps formed 108 HRUs by multiple hydrological response unit method. In this study, SWAT simulated surface runoff using modified SCS curve number method with daily precipitation data. The Penman–Monteith method was used to determine the potential ET for simulating actual ET based on the approach developed by Ritchie (1972), in which evaporation from the soil surface and transpiration from vegetation are simulated separately. Soil water evaporation was estimated as an exponential function of soil depth and water content, based on potential ET and a soil cover index calculated by above ground biomass, confined to the upper limit of 80% of plant available water on a given day. The model was calibrated by optimizing the coefficient of efficiency (Nash and Sutcliffe, 1970). The flow diagram of simulating hydrological process by SWAT is presented in Figure 3.

DOI: 10.1002/hyp

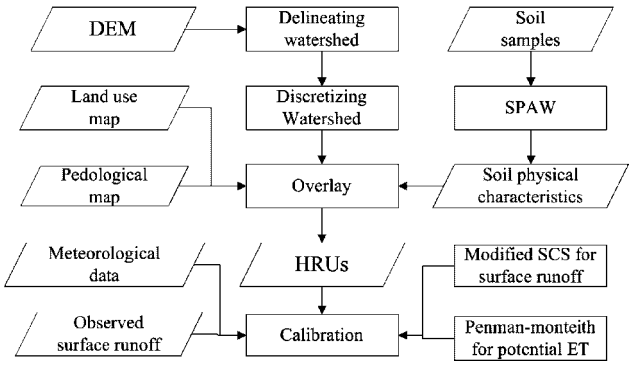

Figure 3. Flow diagram of simulating hydrological processes by SWAT

METHOD AND DATA COLLECTION

To make the comparison as rigorous as possible, the remote sensing-based models and SWAT were tested using a common data set, including the daily precipitation, runoff, daily maximum and minimum temperature, air temperature at the satellite overpass time, daily vapor pressure deficit, daily net radiation, wind speed, land use classification, soil type distribution with its physical properties, Priestly–Taylor parameter, etc. provided from remotely sensed data, 8 meteorological stations and 1 runoff station, and the field campaigns. The instantaneous fluxes were extended to daily ET by assuming the evaporative fraction invariant for comparing with SWAT-based daily ET and examining the underlying physical mechanisms of remote sensing-based models.

Two Landsat5 Thematic Mapper (TM) imageries acquired at 10 : 43 a.m. local time on DOY 174 and DOY 206, 2005, respectively. The meteorological and hydrological data related to this study were collected from the precipitation, runoff and meteorological stations within or near the watershed. Meteorological records show that there is marked contrast in meteorological condition for those two days, large air drying power induced by low air humidity, high air temperature and moderate or high wind speed for DOY 174 but small air drying power for DOY 206. Besides, the absence of rain events for 3 days before DOY 174 and the presence of consecutive rain events from DOY 201 to DOY 204 ultimately resulted in the difference in soil moisture availability across the whole watershed for both imagery-acquired days. TM5 is used to derive the surface characteristics surface albedo, surface emissivity, surface temperature, fractional vegetation cover, vegetation height. DEM provides the parameters of terrain, such as slope, aspect and elevation for computing the radiation. Meteorological data, including wind speed, air temperature and water vapor pressure, are main inputs for computing the surface and aerodynamic resistances. Vegetation and soil parameters are obtained from field campaigns. Vegetation height of sampling positions of each land cover type is used for establishment of the empirical relationship between vegetation height and Soil-adjusted Vegetation Index (SAVI) over the scene. The average leaf width for cropland was set as 0·08 m, 0·05 m for mixed forest and orchard, 0·02 m for conifer, 0·01 m for grassland at the studied period. The roughness length for soil surface was set as 0·01 m. The net radiation with component (vegetation and soil) partition, soil heat flux, vapor pressure deficit, vapour pressure curve slope and surface and aerodynamic resistances is comprised of the common data set for certain remote sensing-based model.

The hydrological processes of the whole 2005 were simulated by SWAT on the daily time step. The calibration was performed by comparing the simulated daily runoff with the observed one and some parameters in SWAT were calibrated in order to improve the efficiency of predictions. Finally, the daily ET values of the whole watershed on DOY 174 and 206 from SWAT were chosen as the basis for accuracy assessment of outputs from remote sensing-based models. Nine soil types, including Grey Forest Soils, Fluvo-Aquic Soils, Skeletol Soils, Aeolian Soils, Chestnut Soils, Alluvial Soils, Cinnamon Soils, Brown Earths, Grey-Cinnamon Soils, were sampled from 25 soil moisture monitoring sites, each of which was representative by three sampling positions, for specifying the percentage of sand, silt and clay, bulk density, organic carbon content, saturated hydraulic conductivity of three stratifications, the topsoil, intermediate layer soil and deep soil, of each sampling position, with soil moisture content obtained on 13 July and 12 August 2005, for one component of calibration for SWAT, totally 450 soil samples collected.

The data sources, including DEM, remotely sensed data, meteorological data, vegetation and soil characteristic parameters, and other parameter/variable derivation related to four remote sensing-based models mentioned in this study are shown in Figure 4.

RESULTS AND DISCUSSION

Overall results

The ET estimates for a wide range of land covers from the single-source models and two-source models for DOY 174 and DOY 206 are shown in Table I, with their frequency distributions shown in Figure 5. As a whole, the ET estimates of the watershed from all these models for DOY 206 are larger than that for DOY 174 because the daily mean net radiation, a key variable affecting the accumulative latent heat flux, for DOY 174 (150·7 W m^{-2}) is lower than that for DOY 206 (194·4 W m^{-2}), with a smaller evaporative fraction for DOY 174 compared with DOY 206, except that generated by P-TSEB (0·643 for DOY 174; 0·642 for DOY 206). The frequency distribution of ET estimates could, to a large extent, reflect the capability of models to signal the variation in soil moisture and vegetation state, two of the main factors affecting the ET distribution. The presence of significant variation in soil moisture (there was no rainfall three days before DOY 174 but consecutive rainfall from DOY 201 to DOY 204) and fractional vegetation cover (0·598 for DOY 174; 0·695 for DOY 206) during the vegetation growing season, combined

DOI: 10.1002/hyp

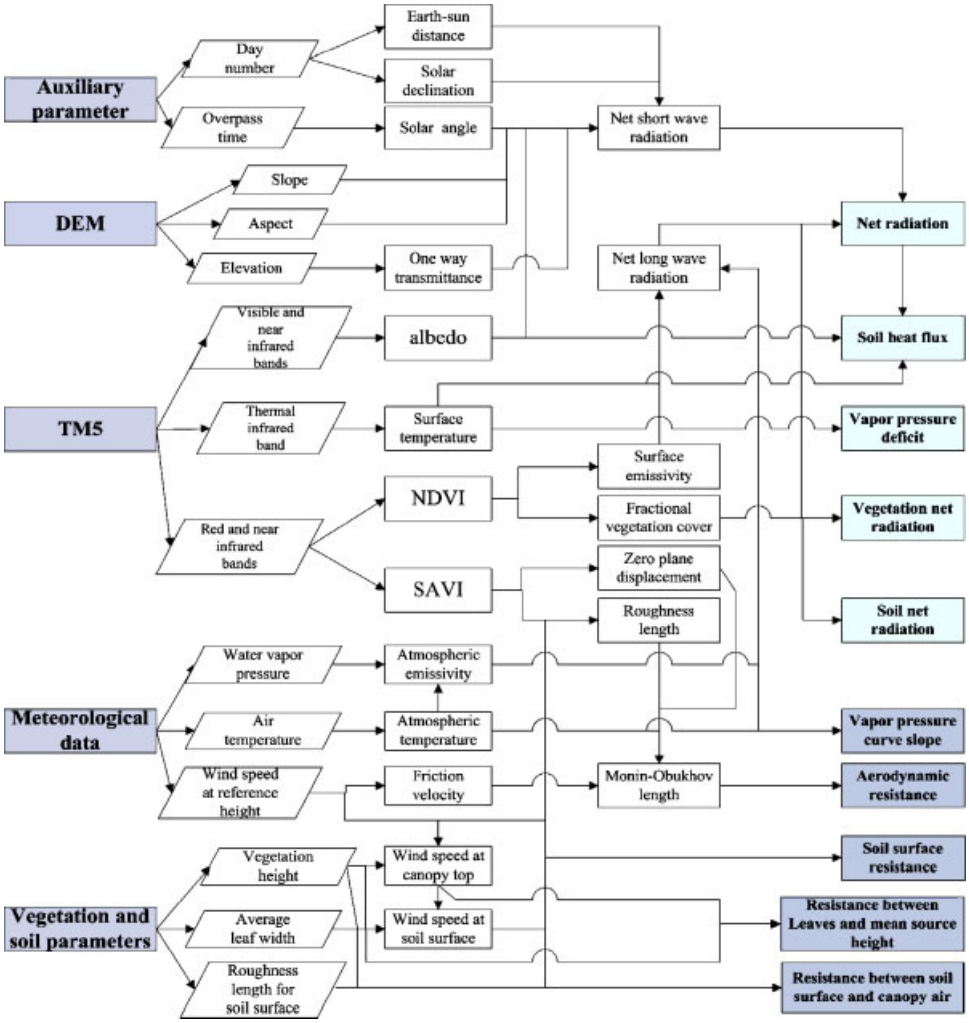

Figure 4. Data sources and flow diagram of derivation of basal parameters/variables. The inputs of remote sensing-based models include the remotely sensed data, digital elevation model (DEM), meteorological data, vegetation and soil parameters and auxiliary parameters

Table I. Daily actual ET of different land use classification from four remote sensing-based models for DOY 174 and DOY 206

Land use (1st level classes)	Land use (2nd level classes)	Number of pixels	Area (%)	SEBAL (mm)		SEBS (mm)		P-TSEB (mm)		S-TSEB (mm)	
				174	206	174	206	174	206	174	206
Cropland	Paddy land	3805	26·8	3·1	5·0	3·7	5·0	4·1	4·9	3·0	5·2
	Flat dry land	170 459		2·3	4·8	3·0	4·8	3·5	4·8	2·3	5·0
	Slope dry land	626 467		2·6	4·6	3·1	4·6	3·5	4·7	2·8	4·9
Woodland	Forest	613 816	54·7	3·5	4·4	3·5	4·3	3·7	4·3	4·0	4·7
	Shrub	690 010		2·9	3·9	3·1	3·9	3·5	4·0	3·5	4·4
	Woods	327 709		2·4	4·1	2·6	4·1	2·9	4·3	3·1	4·5
	Others	1737		2·5	3·5	2·8	3·6	3·4	3·7	3·3	4·2
Grassland	Dense grass	298 837	16·5	3·4	5·2	3·5	5·1	3·6	5·1	3·2	5·3
	Moderate grass	194 489		3·8	5·1	4·0	5·1	4·1	4·9	3·6	5·3
Water body	Reservoir	160	0·6	6·6	5·9	6·7	5·9	6·6	5·9	6·6	5·9
	River-beach	18 528		1·3	3·4	3·5	5·3	1·3	3·4	1·3	3·4
Built-up land	Urban built-up	4682	0·2	0·1	0·0	3·1	3·3	0·1	0·0	0·1	0·0
	Rural area	15 601	0·5	0·1	1·1	2·7	5·0	0·1	1·1	0·1	1·1
Sandy land	Sandy land	14 899	0·5	1·0	0·7	1·9	4·1	1·0	0·7	1·0	0·7
Others		6145	0·2	4·7	5·9	5·1	6·3	4·8	5·9	4·8	5·9
Mean evaporation fraction				0·536	0·637	0·594	0·639	0·643	0·642	0·599	0·686
Mean daily ET of the watershed				2·94	4·39	3·10	4·42	3·47	4·43	3·25	4·73
Standard deviation				1·16	1·04	0·99	0·94	0·97	1·00	1·09	0·84

DOI: 10.1002/hyp

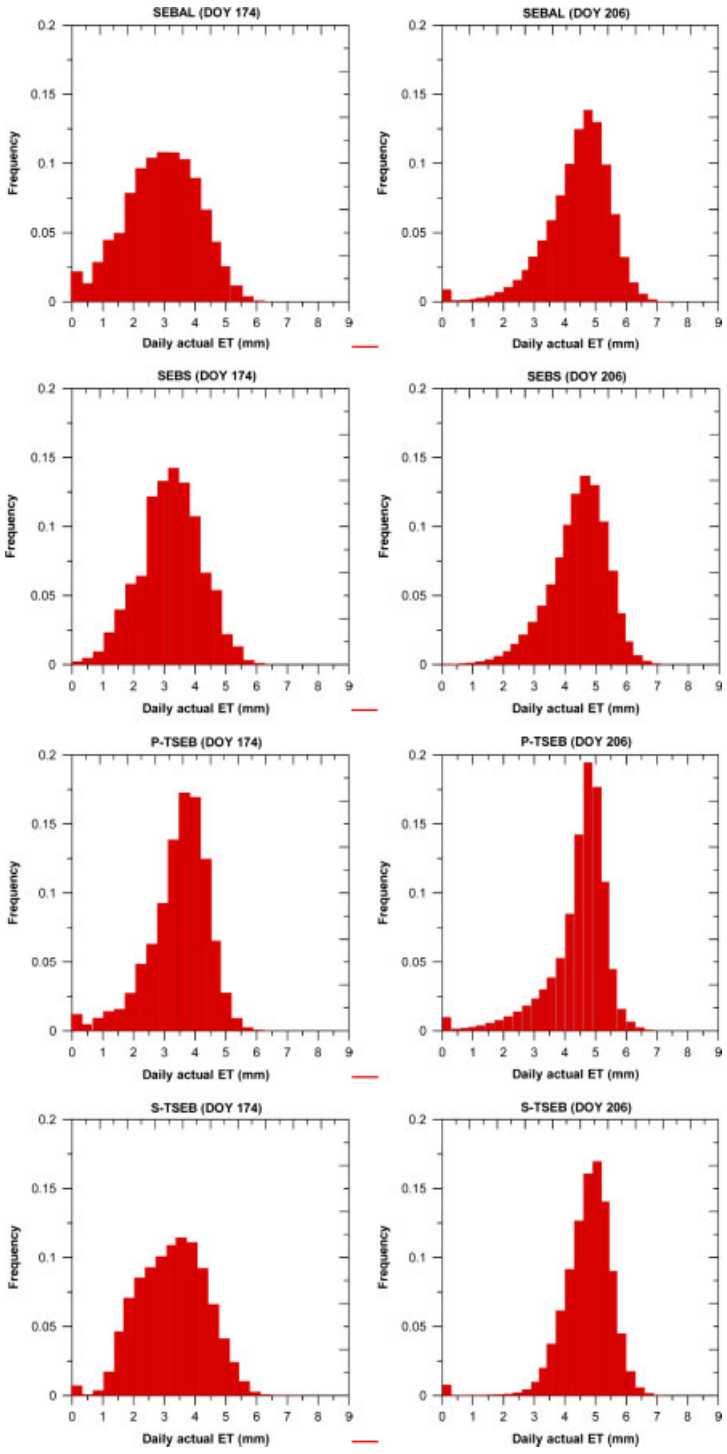

Figure 5. Frequency distributions of ET estimates from four remote sensing-based models of the whole watershed on DOY 174 and DOY 206. A bin size of 0·3 mm day^{-1} was specified. The pixel number and standard deviation are shown in Table I

with the marked contrast in meteorological conditions (wind speed: 2·6 m s^{-1} at the satellite overpass time for DOY 174; 1·2 m s^{-1} for DOY 206; air temperature: 27·7 °C at the satellite overpass time for DOY 174; 25·7 °C for DOY 206; daily mean relative humidity: 61% for DOY 174; 71% for DOY 206), synthetically induced the differences in frequency distribution of ET estimates for both remote sensing imagery-acquired days.

Different models have different capabilities to reflect the difference in frequency distribution of ET estimates, as shown in Figure 5. In principle, the differences between ET distributions from the four studied models for DOY 174 are larger than that for DOY 206 approximating the standard normal distribution, which may result from the marked differences in distribution of soil moisture, fraction vegetation cover and daily mean net radiation across the watershed for DOY 174, while being even distribution for DOY 206 (see Figure 6). It appears that for days of large ET induced by combined effects of high soil moisture availability, high radiation and low wind

DOI: 10.1002/hyp

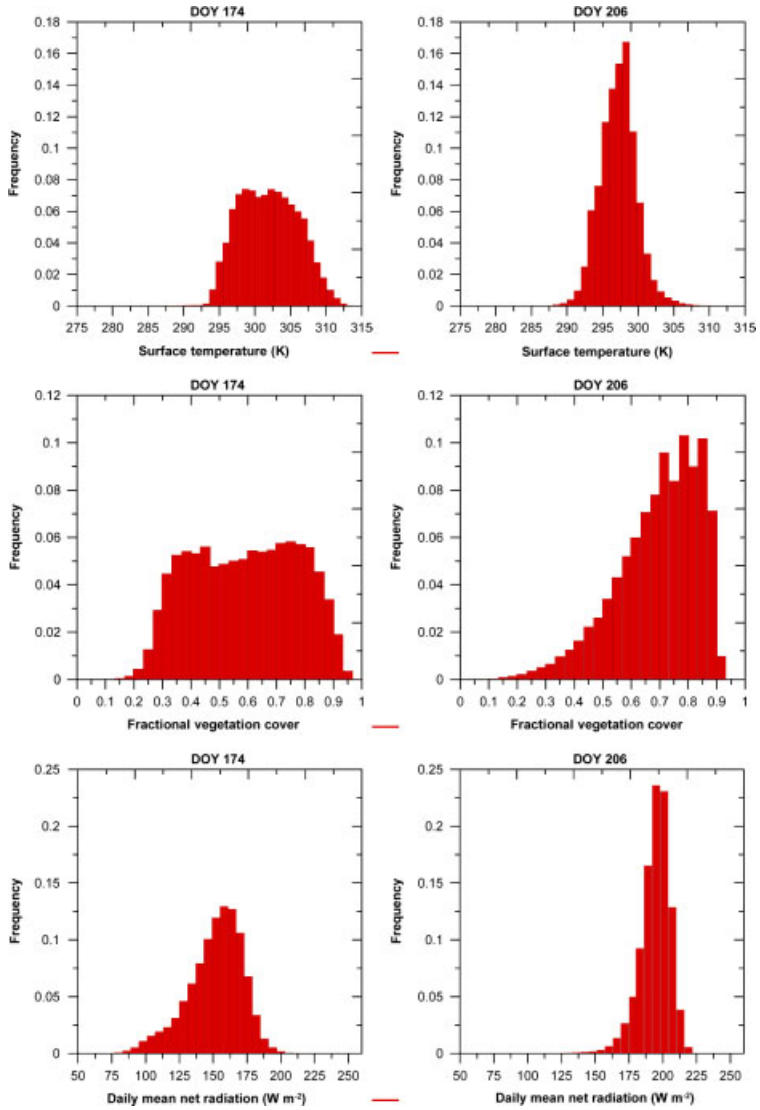

Figure 6. Distributions of remotely sensed surface temperature (K), fractional vegetation cover and daily mean net radiation (W m^{-2}) of the whole watershed for DOY 174 and DOY 206, respectively. A bin size of 1 K for the surface temperature histogram, 0·03 for fractional vegetation cover, and 5 W m^{-2} for daily mean net radiation were specified

speed, the frequency distribution of ET estimates from the single-source and two- source models are similar, but could show significant dissimilarity for those days having small ET.

SEBAL and SEBS

For vegetation cover, such as the cropland, woodland and grassland, the differences in ET estimates between SEBAL and SEBS are more distinct for DOY 174 compared with DOY 206. Because the soil heat flux from the SEBS algorithm is larger than that from SEBAL (SEBAL 81·8 W m^{-2}; SEBS 111·5 W m^{-2} for DOY 174; SEBAL 62·9 W m^{-2}; SEBS 93·8 W m^{-2} for DOY 206), the soil heat flux from SEBS was substituted for that from SEBAL to isolate the difference in parameterization of sensible heat flux from the difference in specification of soil heat flux, and then both models were run using identical soil heat flux. The sensible heat flux from SEBAL is larger than that from SEBS, but the exceeded magnitude for DOY 174 differs from that for DOY 206 (ΔH 34·8 W m^{-2} for DOY 174; ΔH 11·3 W m^{-2} for DOY 206), which could be explained by the difference in treatment of the KB^{-1} parameter in the two models. In SEBAL, KB^{-1} is taken to be a constant value of 2·3 applied over the entire scene, namely z_h is 1/10 of z_m, whereas KB^{-1} is a distributed parameter in SEBS. In this study, the mean KB^{-1} over the scene for DOY 174 and DOY 206 was 3·005 and 2·333, respectively, slightly larger than the nominal value of 2·3 in SEBAL but leading to the discrepancies in computation of sensible heat flux, specifically for the sparsely cover and non-evaporative area, such as the built-up land and sandy land, under large drying power and low soil moisture conditions (e.g. paddy land: ΔET 0·6 mm between SEBAL and SEBS for DOY 174; ΔET 0 mm for DOY 206; flat dry land: ΔET 0·7 mm for DOY 174 and 0 mm for DOY 206). A larger KB^{-1} parameter corresponds to larger resistance to heat transfer, thereby yielding lower sensible heat flux values (SEBAL 287·7 W m^{-2}; SEBS 252·9 W m^{-2} for

DOI: 10.1002/hyp

DOY 174; SEBAL 235·2 W m^{-2}, SEBS 223·9 W m^{-2} for DOY 206). For non-evaporative areas, a noticeable difference in sensible heat flux estimates between SEBAL and SEBS was revealed (SEBS produced illogical larger ET estimates for sandy land and built-up land for both DOY 174 and 206). The conclusion could be drawn that the single-source model is highly sensitive to the KB^{-1} parameter, namely the roughness length for heat transfer.

P-TSEB and S-TSEB

For vegetation cover, with the exception of forest and woods, ET estimates from P-TSEB are larger than those from S-TSEB for DOY 174, and lower than those from S-TSEB for DOY 206, exhibiting a larger difference in ET amount for DOY 174 compared with DOY 206. Moreover, the differences in ET estimates between the two models decrease with fractional vegetation cover (e.g. paddy land: ΔET 1·1 mm; slope dry land: ΔET 0·7 mm for DOY 174; paddy land: ΔET 0·3 mm; slope dry land: ΔET 0·2 mm for DOY 206). The reason why the differences in ET estimates from P-TSEB and S-TSEB are smaller for low fractional vegetation cover and/or cover in dry environments than for high fractional vegetation cover and/or cover in wet environments may be the difference in their resistance networks. S-TSEB has two sets of resistances across which sources parameterization is applied assuming the exchange of component sensible and latent heat fluxes take place within the canopy atmosphere layer at the in-canopy source height, where the resistances meet, to allow interaction between the land surface and the local atmosphere. However, there is no heat fluxes exchange existing between soil and vegetation in P-TSEB. The differences in component sensible heat fluxes between P-TSEB and S-TSEB for DOY 174 (P-TSEB: H_c 97·5 W m^{-2}; H_s 121. 4 W m^{-2}; S-TSEB: H_c 51·4 W m^{-2}; H_s 192·8 W m^{-2}) are larger than those for DOY 206 (P-TSEB: H_c 142·5 W m^{-2}; H_s 86·1 W m^{-2}; S-TSEB: H_c 109·2 W m^{-2}; H_s 89·5 W m^{-2}), which would be induced by the difference in parameterization of resistance networks under different meteorological conditions. In addition, the evaporative fraction from P-TSEB for DOY 174 is slightly larger than that for DOY 206, contrary to the identical tendency of larger evaporative fraction from single-source models and S-TSEB for DOY 206, thus lending less credibility to application of P-TSEB to large air drying power condition. Consequently, the fractional vegetation cover and vegetation architecture, manner of resistance network and meteorological condition synthetically determine the partition of net radiation, rendering discrepant performance between P-TSEB and S-TSEB.

Discussion of results

The surface temperature, fractional vegetation cover, roughness length for momentum transport and daily mean net radiation for DOY 174 and DOY 206 were selected to analyse the variation in ET estimates of various land covers, as provided in Table I. The ET estimates shown in Table I and variable/parameter estimates shown in Table II explicitly illustrate the following. (1) The larger ET estimates to a large extent correspond to the lower surface temperature and larger daily mean net radiation if there is no notable difference in roughness length for momentum transfer. For instances, paddy land has the lowest surface temperature and largest daily mean net radiation, hence showing largest ET estimates from all the models in cropland classification for both days. Forest land has the lowest surface temperature for both days, thus exhibiting the largest ET estimates in the woodland classification despite its daily mean net radiation being slightly lower than that of other land use classifications for DOY 206. Owing to assimilation of the surface temperature to compute the sensible heat flux, both single-source and two-source models can produce reasonable ET distribution over a wide range of land covers at the watershed scale. (2) In general, the fractional vegetation cover significantly affects the surface temperature, that is, higher fractional vegetation cover tends to show lower surface temperature, but exceptions were observed. For instances, the fractional vegetation cover of paddy land (0·37) was lower than dry land for DOY 174, while paddy land showed the lowest surface temperature, exhibiting larger ET estimated from both single-source and two-source models, which may result from the difference in soil moisture condition. Therefore, it seems logical that the surface temperature synthetically can reflect

Table II. Key variables, surface temperature, fractional vegetation cover, roughness length for heat transfer, and daily mean net radiation significantly affecting the daily actual ET for DOY 174 and DOY 206

Land use (1st level classes)	Land use (2nd level classes)	T_{sur} (K)		f_c		z_m (m)		R_{day} (w m^{-2})	
		174	206	174	206	174	206	174	206
Cropland	Paddy land	304·5	297·3	0·370	0·654	0·04	0·11	162·4	199·9
	Flat dry land	306·5	298·5	0·359	0·616	0·04	0·09	144·5	199·6
	Slope dry land	304·7	298·8	0·442	0·607	0·05	0·08	146·0	197·9
Woodland	Forest	298·7	295·2	0·736	0·782	0·21	0·25	158·8	191·3
	Shrub	300·5	296·7	0·652	0·733	0·18	0·23	153·8	192·4
	Woods	301·7	296·5	0·668	0·731	0·18	0·23	142·6	192·4
	Others	301·4	297·0	0·617	0·759	0·16	0·23	156·5	192·4
Grassland	Dense grass	302·5	297·6	0·583	0·680	0·04	0·05	145·2	194·4
	Moderate grass	302·4	298·7	0·532	0·654	0·03	0·05	160·5	198·1

DOI: 10.1002/hyp

the combined effects of soil moisture availability, fractional vegetation cover and terrain on heat flux exchanges between land surface and atmosphere. (3) Although the surface temperature of grassland was higher than that of woodland, the larger ET estimates of grassland from all models compared with woodland demonstrate that the roughness length for momentum transfer also plays an extremely important role in computation of resistances. Larger roughness length for momentum transfer, also associated with larger roughness length for heat transfer, can together decrease the resistance to sensible heat exchange, and therefore exhibit larger sensible flux. In fact, some researchers have carried out sensitivity analyses with respect to the parameters of the single-source and two-source models. For example, Zhan *et al*. (1996) pointed out that the single-source models are very sensitive to the roughness length for momentum transfer, and the surface temperature significantly affects the amount of sensible heat flux for both single-source and two-source models. Timmermans *et al*. (2007) also stated that both P-TSEB and SEBAL rely heavily on the remotely sensed surface temperature, and the output from P-TSEB is also significantly influenced by the frictional vegetation cover. Therefore, it appears that the surface temperature, fractional vegetation cover, roughness length for momentum transfer and the daily net radiation significantly determine the amount and distribution of ET estimates.

In conclusion, the single-source and two-source models have the capability to capture the essential trend in ET distribution over a variety of land covers, although there are differences in their predictions under complex underlying surface and different meteorological conditions.

Results from SWAT

The daily simulated and measured runoffs with the rainfall occurrence of the whole watershed from 1 June (DOY 152) to 31 August (DOY 242) are shown in Figure 7. The simulated daily potential ET and actual ET of the whole watershed with daily sunshine duration at the same period are shown in Figure 8. The correlation coefficient (R^2), coefficient of efficiency (E_{ns}) value and relative error (R_e) are 0·935, 0·870 and 16·2%, respectively, indicating high accuracy of the simulated hydrological processes of the watershed during this period.

Figure 7 illustrates that the measured runoff at the outlet of the watershed has a rapid response to the rainfall, which could be explained by the reason of short concentration time induced by steep slopes and short slope lengths of sub-basins for the watershed. The runoff was generally low because of the low rainfall and small curve number values in terms of land covers and soil types specified by SWAT during that period. The simulated runoff is generally accordant with the observed values except for those extreme rainfall events on DOY 179 and 180 being not present the surface runoff lag, DOY 201 and 221 with larger predictions, and a short period prior to DOY 186 and after DOY 236 with little rainfall. Even though SWAT has the capability to accurately capture the distribution of daily runoff over a long period, it could not predict some extreme flow events primarily due to the rainfall representation of limited stations and the subdaily variation in rainfall intensity that could not be captured by the SCS method on the daily step. The potential ET can reflect the combined effects of meteorological factors on actual ET and can be considered the upper limit of actual ET (also see Figure 8). The rain occurrence and actual sunshine duration could to some extent signal the evaporation trend. Figure 7 and Figure 8 illustrate explicitly that (1) the potential ET largely depends on the sunshine duration, namely, the daily net radiation; (2) the counterintuitive events, such as 31·7 mm rainfall with 7·2 h sunshine on DOY 179, 18·0 mm rainfall with 7·1 h sunshine on DOY 201 and 21·5 mm rainfall with 3·7 h sunshine on DOY 212, respectively, could be induced by the subdaily variation in meteorological condition; (3) in principle, there is a time-lag between rainfall and actual ET. The actual ET of DOY 205, 206, 207 are larger than those of other days in July because of the higher soil moisture availability and larger daily net radiation after consecutive rainy days from DOY 201 to DOY 204.

In conclusion, the simulated hydrological processes are in accordance with reality and the simulated actual ET of the whole watershed on DOY 174 and 206 could

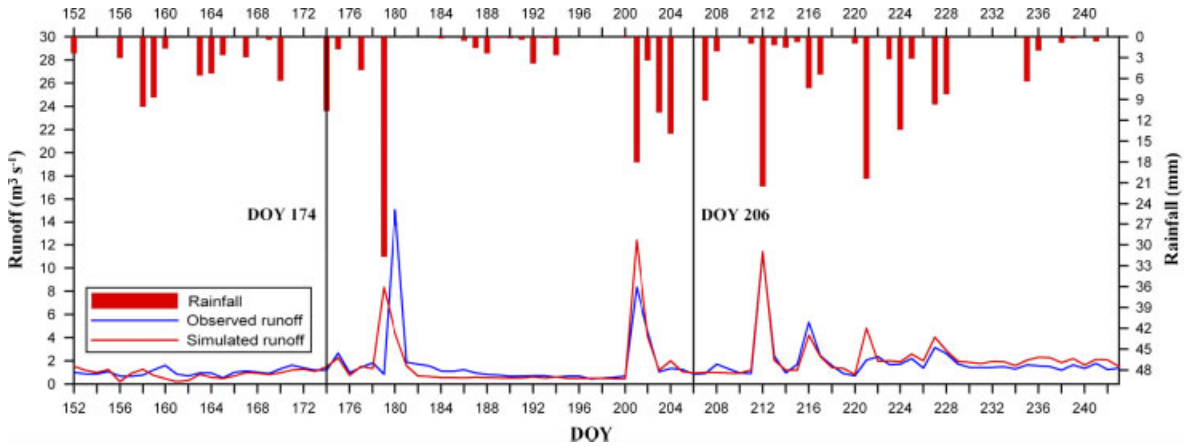

Figure 7. Simulated and measured runoff (m^3 s^{-1}) for Dage gauging station with the daily rainfall (mm) from DOY 152 to DOY 243

DOI: 10.1002/hyp

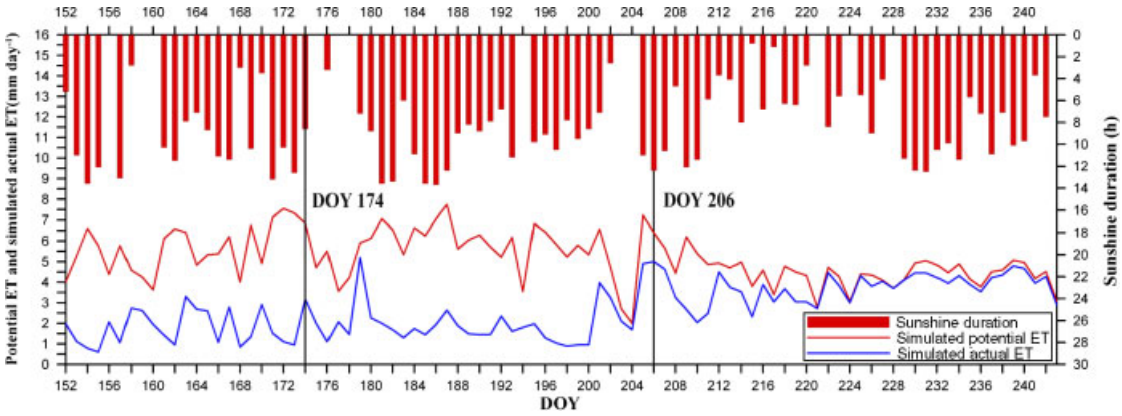

Figure 8. Simulated daily potential ET (mm) and actual ET (mm) of the whole watershed with the daily sunshine duration from DOY 152 to DOY 243, 2005. The daily actual ET on DOY 174 and DOY 206 were selected from the credible hydrological processes simulated by SWAT as the criterion for making an accuracy assessment of ET estimates from remote sensing-based models

Table III. Relative error of ET estimates from remote sensing models versus SWAT

Model	SEBAL		SEBS		P-TSEB		S-TSEB		SWAT	
DOY	174	206	174	206	174	206	174	206	174	206
ET(mm)	2·94	4·39	3·10	4·42	3·47	4·43	3·25	4·73	3·18	5·01
Relative error (%)	−7·5	−12·4	−2·5	−11·8	9·12	−11·6	2·2	−5·6	—	—

be used as criteria for accuracy assessment of remote sensing-based models. The relative errors of each remote sensing-based ET versus SWAT-based ET on DOY 174 and 206 are shown in Table III.

Uncertainties concerning the assumption of negligible net groundwater flow out of the watershed, errors in the hydro-meteorological records, errors induced by spatial interpolation of meteorological variables are hard to quantify and are not discussed in this paper. Assuming all of these uncertainties are negligible, the ET estimates from S-TSEB have higher accuracy and relatively reasonable ET distribution. Thus, S-TSEB was selected to be the basis for making an intercomparison with other remote sensing-based models.

ASSESSMENT AND INTERCOMPARISON

The intercomparison of ET estimates from SEBAL, SEBS and P-TSEB versus S-TSEB for DOY 174 and DOY 206 was performed to examine the utilities and limitations of models over a wide range of land covers and meteorological conditions. The ET samples of each land cover from SEBAL, SEBS, and P-TSEB versus S-TSEB extracted randomly from the scene are shown as scatter plots, showing explicitly the differences between them (Figures 9 and 10). The correlation coefficient (R^2), root mean squared error (RMSE), mean absolute percentage difference (MAPD), slope of the linear regression (Slope) and intercept of the linear regression (Intercept) were selected for assessing results (also see Table IV and Table V).

Single-source models

Overall, SEBAL yielded lower RMSD and MAPD over high-cover areas such as paddy land, forest and dense grass compared with dry land, woods and moderate grass, with reference to ET estimates from S-TSEB for both days. The magnitude of RMSD and MAPD for woodland (MAPD 16·19% and 26·22% for forest and woods on DOY 174, respectively; 6·11% and 9·11% on DOY 206) is larger than that for cropland and grassland. Moreover, the RMSD and MAPD of SEBAL versus S-TSEB for various land covers for DOY 174 were larger than that for DOY 206. With regard to SEBS statistics, it is clear, for DOY 206, that the RMSD and MAPD of various land covers presented a tendency similar to SEBAL, with larger differences across lower vegetation cover (dry land, woods), while for DOY 174, compared with woodland and grassland, SEBS generated larger differences over cropland with MAPD up to 20% and RMSD approximate 0·6 mm, with slightly larger MAPD for paddy land (26·56%) than dry land (20·86%). In addition, SEBAL and SEBS generated lower MAPD of grassland within 10% for both days, SEBS showing slightly larger values. In general, SEBAL yielded lower values of RMSD and MAPD of various land covers for both days compared with SEBS, with the exception of slightly larger MAPD for forest (SEBAL 16·19%; SEBS 13·18%) and woods (SEBAL 26·22%; SEBS 20·96%) for DOY 174. Consequently, the performances of single-source models varied with land cover and different mechanisms of water–heat transfer and meteorological conditions, appearing more applicable to dense canopy and humid environments. Larger RMSD and MAPD from SEBAL versus S-TSEB of woodland

DOI: 10.1002/hyp

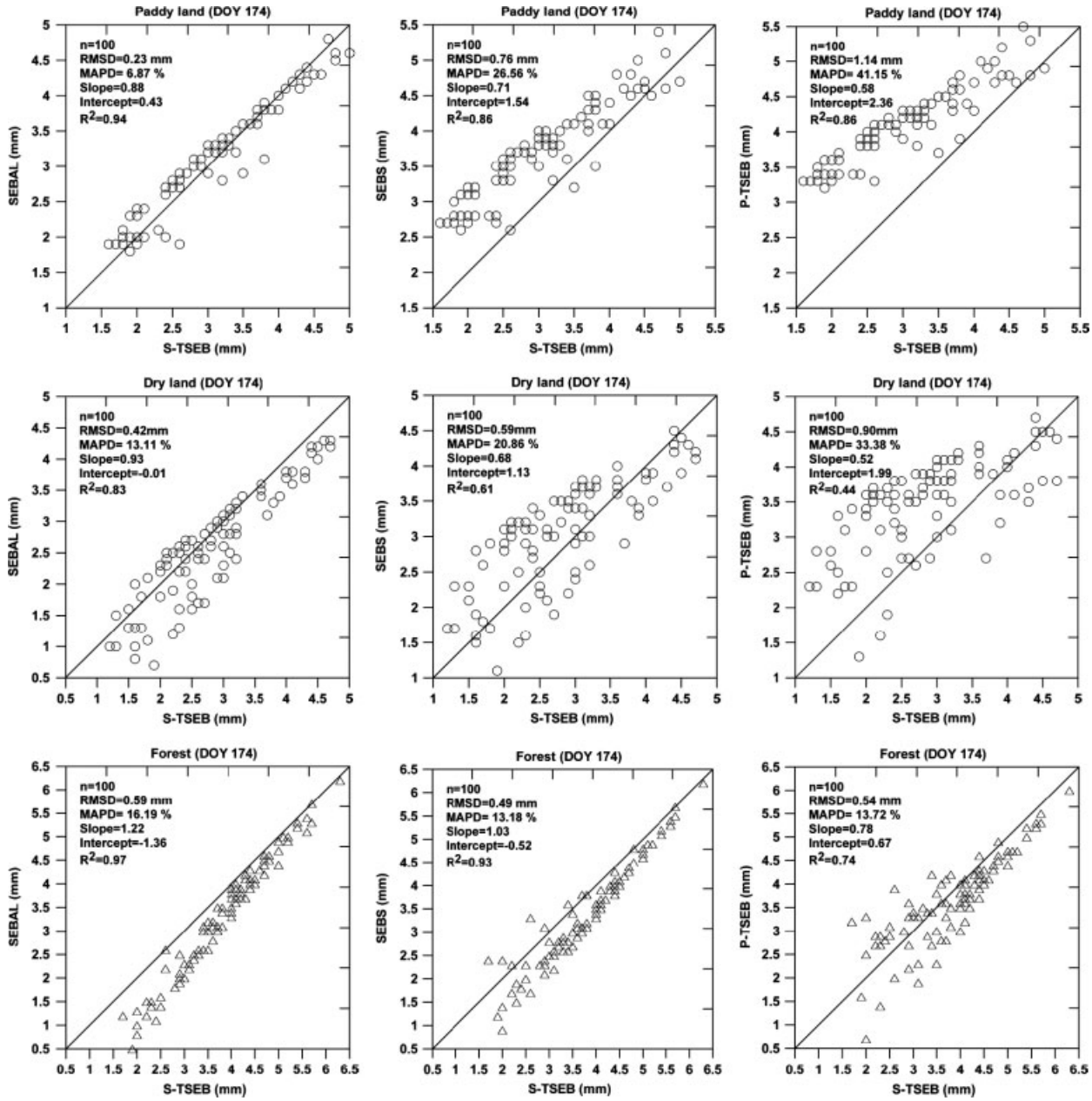

Figure 9. Scatter plots of daily actual ET from SEBAL, SEBS and P-TSEB versus S-TSEB for various land coves across the watershed for DOY 174, with the statistics, including number of samples (n), root mean squared error (RMSE), mean absolute percentage difference (MAPD), slope of the linear regression (Slope), intercept of the linear regression (Intercept) and correlation coefficient (R2), presenting in each scatter plot and Table IV

for both days may be induced by the complexity in the underlying surface, comprised of conifer, broadleaf, and mixed forest with varying fractional vegetation cover and architecture, which renders SEBAL unable to depict turbulent exchanges, and thus degrades the accuracy in ET estimates; the same reason for the application of SEBAL and SEBS to other sparse cover.

The single-source model regards the energy interface of the soil–vegetation–atmosphere continuum as a 'big leaf', without depicting the contribution of vegetation and soil to the total fluxes separately. There is an assumption in the single-source model that the turbulent exchange height for water and heat are uniform with nearly saturated water vapour pressure at leaf surfaces, presenting identical temperatures and resistances for sensible and latent heat flux transfer, which is appropriate for closed-canopy vegetation but may lead to errors in sparse cover. For instance, if the soil surface is very dry and fractional vegetation cover is very low, the sensible heat source is always on the soil surface whereas the water vapour source is close to the canopy. Thus the simplification of the processes of water–heat transfer under sparse canopy cover may result in the deviation from reality.

For SEBAL and SEBS, the latent heat flux is calculated as the residual in the energy balance equation to circumvent the problem related to lack of information on the surface resistances, but the issue of specifying the roughness length for heat transfer, namely the resistance for sensible heat flux, is inevitable. For SEBAL,

DOI: 10.1002/hyp

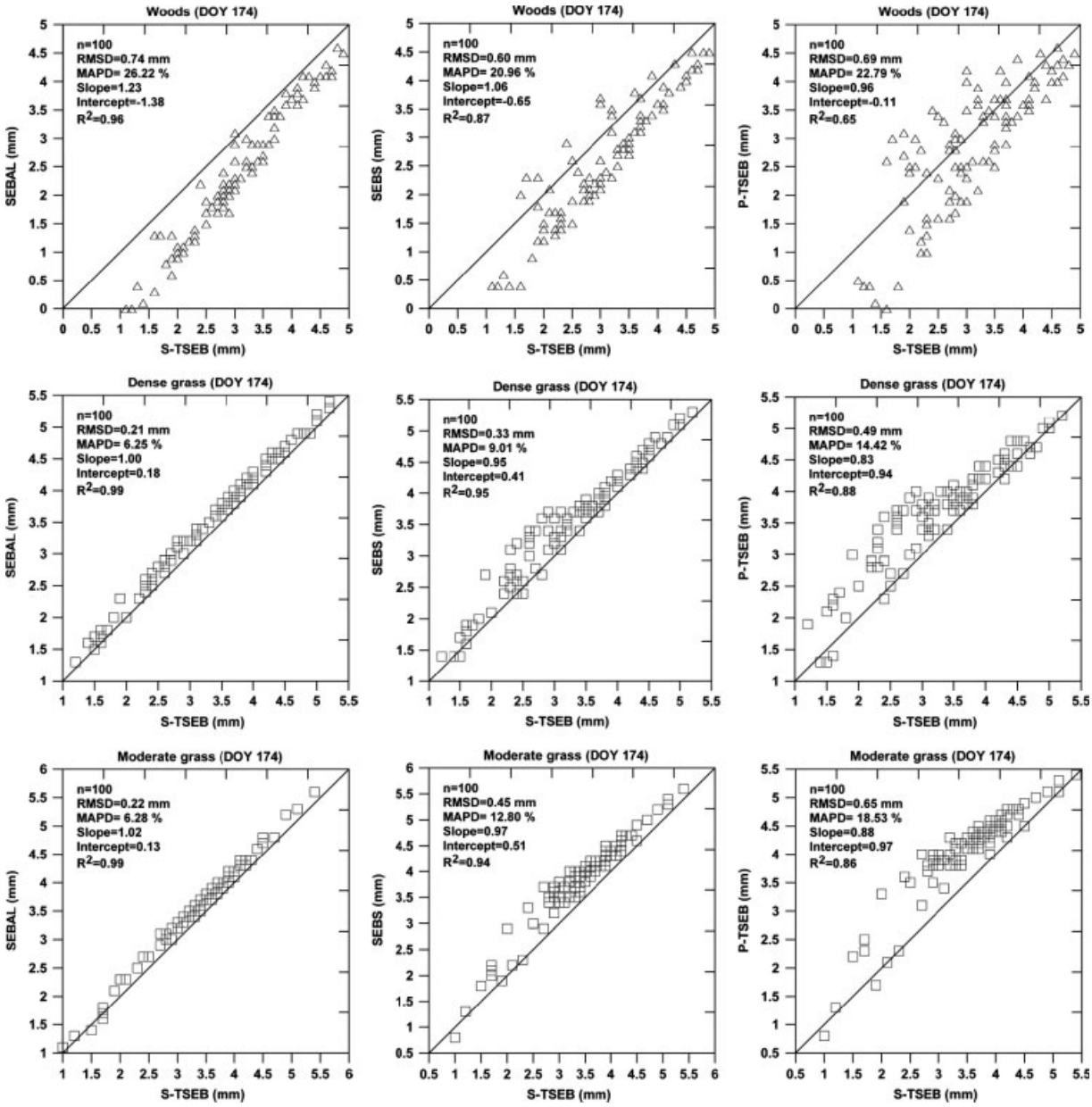

Figure 9. (*Continued*)

a nominal KB^{-1} of 2·3 is applied over the entire scene. The aerodynamic temperature is considered proportional to the satellite-based surface temperature, inferred by the coldest pixel and the warmest pixel, which is a subjective decision in the selection of them because of the confusion from thin cloud, water vapour, etc. across the whole scene. Furthermore, as Verhoef *et al*. (1997) indicated, the widely used KB^{-1} value of 2·3 is too low in most cases, although SEBAL assumes that deviations of actual z_h from the nominal value of $KB^{-1} = 2{\cdot}3$ are absorbed into the calibrated regression equation, which may be the primary source of errors of SEBAL in the estimation of ET over woods comprised of varying vegetation types and structures, especially for large air drying power conditions.

For SEBS, the KB^{-1} parameter is distributed accounting for the characteristics of vegetation, soil, and ambient environment, to depict the influences of differences in underlying surface and surface sub-layer characteristics on the resistance to heat transfer. However, in this study, the discrepancies in ET estimates between SEBS and S-TSEB are actually larger than SEBAL, except estimates of woodland for DOY 174 and dry land for DOY 206. This suggests that SEBS could not improve the performance markedly over complex underlying surfaces if the distribution of meteorological variables, such as relative humidity, air temperature and wind speed required in SEBS cannot be accurately simulated and/or the variables of underlying surface, such as leaf width, heat transfer coefficient of leaf sensitive to estimate the KB^{-1} parameter, cannot be appropriately specified. This is in accordance with the conclusion drawn by Verhoef *et al*. (1997) that calculated KB^{-1} is very sensitive to measuring errors in the micrometeorological variables.

DOI: 10.1002/hyp

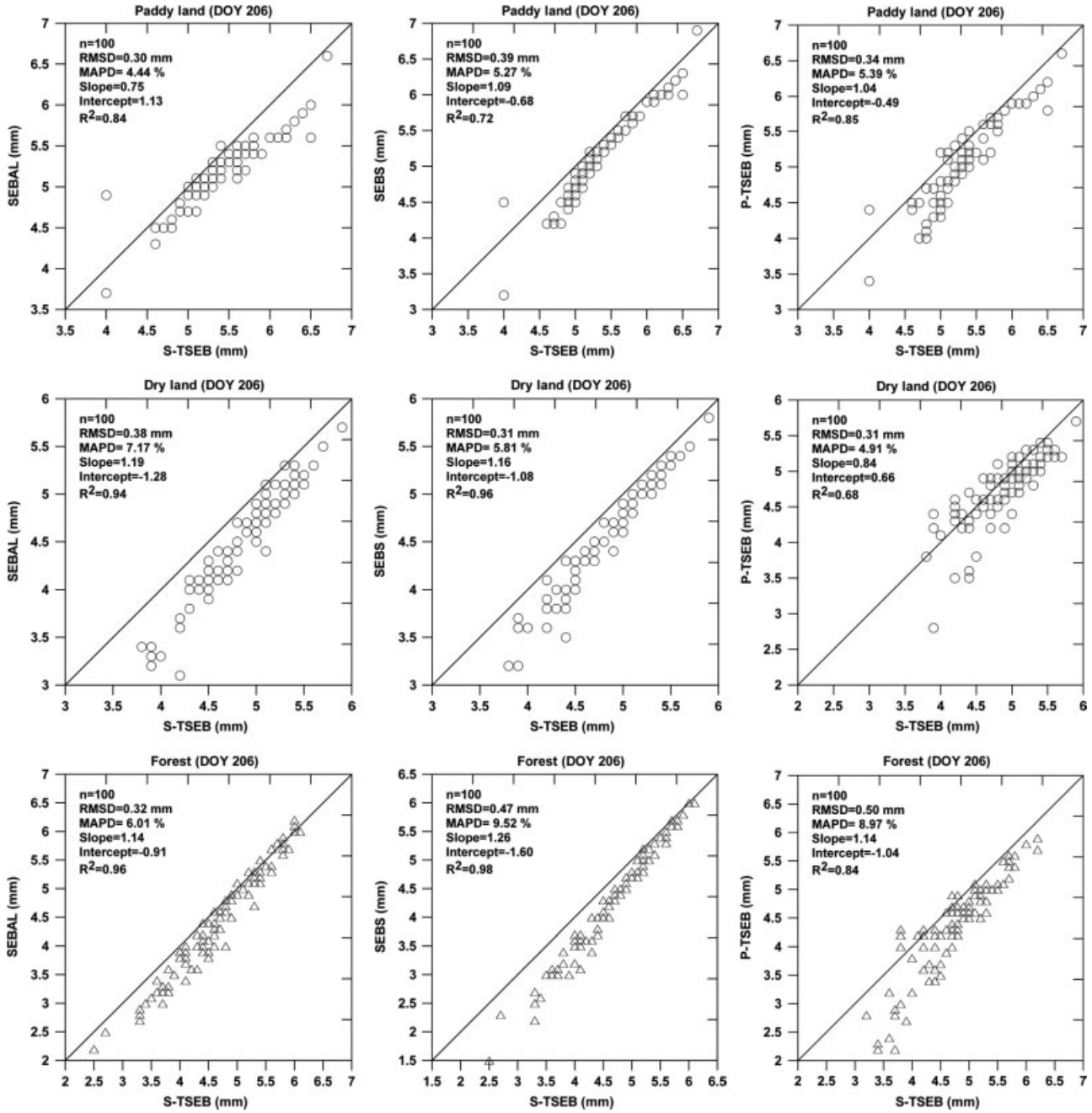

Figure 10. Scatter plots of daily actual ET from SEBAL, SEBS and P-TSEB versus S-TSEB of various land coves in the watershed for DOY 206, with the statistics, including number of samples (n), root mean squared error (RMSE), mean absolute percentage difference (MAPD), slope of the linear regression (Slope), intercept of the linear regression (Intercept) and correlation coefficient (R^2), presenting in each scatter plot figure and Table V

Two-source models

Although P-TSEB generally maintained consistency with S-TSEB in moist air and less contrast in soil moisture availability circumstances, specifically for DOY 206 in this study, presenting low RMSD within 0·5 mm and MAPD within 9% across all land covers, especially lower for dry land, woods and moderate grass of lower fractional vegetation cover, P-TSEB generated MAPD of up to 41·15% of paddy land, with large MAPD reaching on the order of approximately 20% across other land covers and low R^2 of dry land (0·44) and woods (0·65) under large air drying power and marked contrast in soil moisture condition for DOY 174. It seems that P-TSEB is closely in line with S-TSEB over low cover areas under small air drying power and less contrast in soil moisture conditions, whereas it yields large discrepancies under large air drying power and noticeable contrast in soil moisture circumstances, in particular for low cover areas. Therefore, the performances and applicability of P-TSEB relies not only on the characteristics of the underlying surface (fractional vegetation cover, contrast in soil moisture), but also on meteorological conditions.

Under small air drying power and adequate soil moisture conditions, soil heat flux couples to vegetation heat flux weakly, thus the series resistance network

DOI: 10.1002/hyp

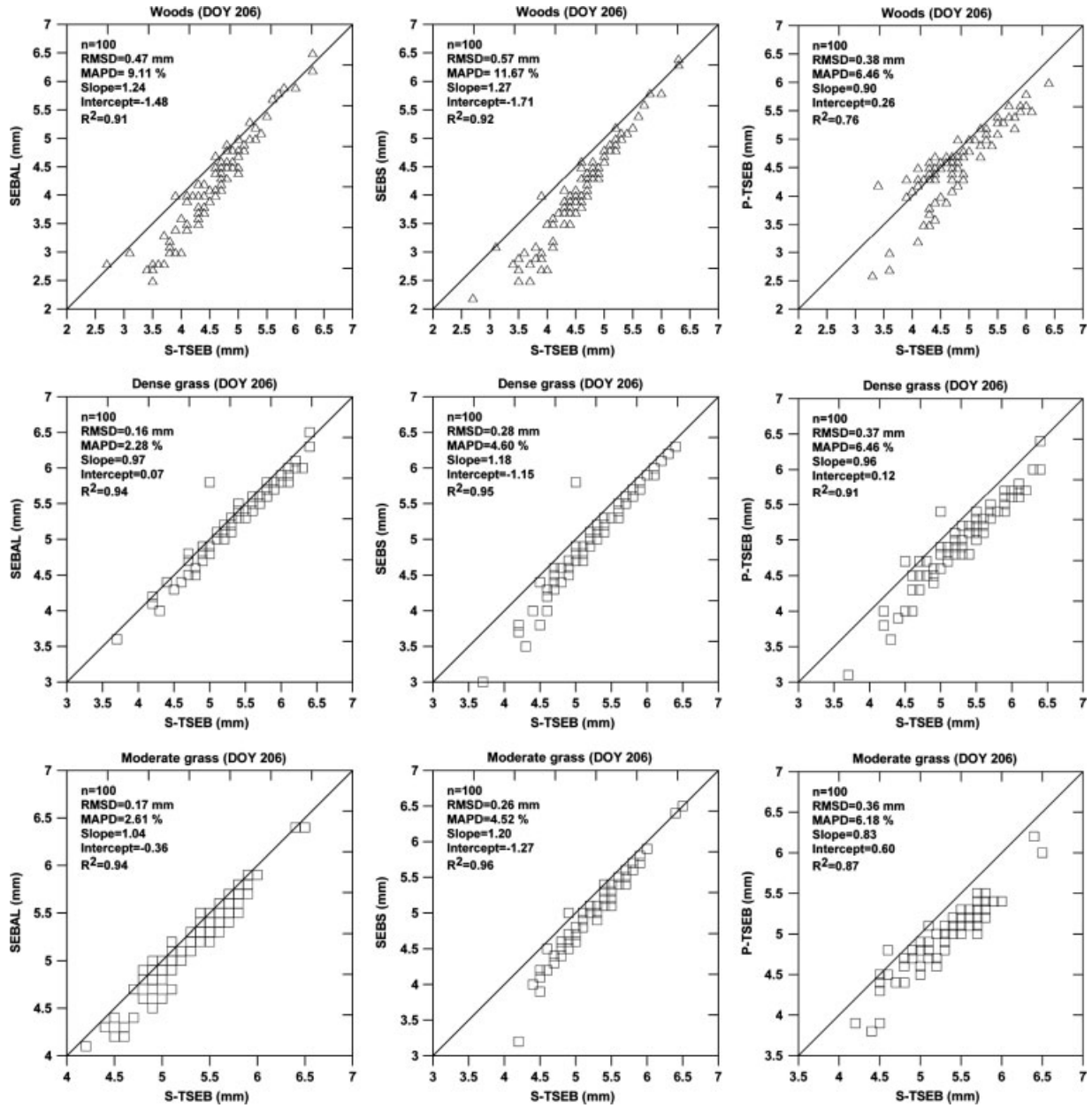

Figure 10. (*Continued*)

gradually degenerates into a parallel resistance network, especially for sparse cover. Nevertheless, for large air drying power and marked contrast in soil moisture conditions, the presence of component coupling makes the two resistance networks distinct, presenting large discrepancies in heat flux estimates between parallel and series parameterization schemes.

CONCLUSIONS

The accuracy assessment in this study is based on the following reasoning and judgments.

(1) SWAT could provide realistic ET amount of a watershed.
(2) Remote sensing-based models using high resolution data could generate reasonable ET distribution
(3) If the ET amount from a remote sensing-based model of a watershed is in agreement with that from SWAT, the remote sensing-based model is believed to have the ability to generate reliable ET amounts at pixel scale. The ET estimates from both methodologies are comparable, which suggests that hydrological model could provide an effective method for accuracy assessment of remote sensing-based models, and moreover, implies a promising direction to address the important problem of temporal extension for practical application of remote sensing-based models to no-imagery days.

The ET estimates from S-TSEB of the studied watershed have the highest accuracy, with relative errors of 2·2% and −5·6% referred to 3·18 mm and 5·01 mm from SWAT for DOY 174 and 206, respectively. Thus S-TSEB.

DOI: 10.1002/hyp

Table IV. Summary statistics of the assessment of SEBAL, SEBS, and P-TSEB with reference to S-TSEB for various land coves on DOY 174

Model		Land cover					
	Statistics N = 100	Paddy land	Dry land	Forest	Woods	Dense grass	Moderate grass
SEBAL	RMSD (mm)	0·23	0·42	0·59	0·74	0·21	0·22
	MAPD (%)	6·87	13·11	16·19	26·22	6·25	6·28
	Slope	0·88	0·93	1·22	1·23	1·00	1·02
	Intercept	0·43	−0·01	−1·36	−1·38	0·18	0·13
	R^2	0·94	0·83	0·97	0·96	0·99	0·99
SEBS	RMSD (mm)	0·75	0·59	0·49	0·60	0·33	0·45
	MAPD (%)	26·56	20·86	13·18	20·96	9·01	12·80
	Slope	0·71	0·68	1·03	1·06	0·95	0·97
	Intercept	1·54	1·13	−0·52	−0·65	0·41	0·51
	R^2	0·86	0·61	0·93	0·87	0·95	0·94
P-TSEB	RMSD (mm)	1·14	0·90	0·54	0·69	0·49	0·65
	MAPD (%)	41·15	33·38	13·72	22·79	14·42	18·53
	Slope	0·58	0·52	0·78	0·96	0·83	0·88
	Intercept	2·36	1·99	0·67	−0·11	0·94	0·97
	R^2	0·86	0·44	0·74	0·65	0·88	0·86

Table V. Summary statistics of the assessment of SEBAL, SEBS, and P-TSEB with reference to S-TSEB for various land coves on DOY 206

Model		Land cover					
	Statistics N = 100	Paddy land	Dry land	Forest	Woods	Dense grass	Moderate grass
SEBAL	RMSD (mm)	0·30	0·38	0·32	0·47	0·16	0·17
	MAPD (%)	4·44	7·17	6·01	9·11	2·28	2·61
	Slope	0·75	1·19	1·14	1·24	0·97	1·04
	Intercept	1·13	−1·28	−0·91	−1·48	0·07	−0·36
	R^2	0·84	0·94	0·96	0·91	0·94	0·94
SEBS	RMSD (mm)	0·39	0·31	0·47	0·57	0·28	0·26
	MAPD (%)	5·27	5·81	9·52	11·67	4·60	4·52
	Slope	1·09	1·16	1·26	1·27	1·18	1·20
	Intercept	−0·68	−1·08	−1·60	−1·71	−1·15	−1·27
	R^2	0·72	0·96	0·98	0·92	0·95	0·96
P-TSEB	RMSD (mm)	0·34	0·31	0·50	0·38	0·37	0·36
	MAPD (%)	5·39	4·91	8·97	6·46	6·46	6·18
	Slope	1·04	0·84	1·14	0·90	0·96	0·83
	Intercept	−0·49	0·66	−1·04	0·26	0·12	0·60
	R^2	0·85	0·68	0·84	0·76	0·91	0·87

SEABL, SEBS and P-TSEB can give similar ET distributions and amounts for DOY 206, but show noticeable discrepancies versus S-TSEB for DOY 174, especially for sparse cover or those land covers having varying types and architectures.

The single-source models are very sensitive to KB^{-1} parameter, rendering marked differences in heat flux estimates under different treatment of roughness length for heat transfer. SEBAL yielded MAPD versus S-TSEB within 26·22% for DOY 174 and 9·11% for DOY 206, large values occurring across low cover and complex underlying surface. SEBS presented MAPD within 26·56% for DOY 174 and 11·69% for DOY 206, respectively, indicating that the accuracy of ET estimates from SEBS could not be markedly improved if meteorology and underlying surface variables could not be accurately simulated or appropriately specified (as required by its KB^{-1} algorithm). As a whole, the single-source models could be more appropriate when applied to higher cover and soil moisture availability areas under small air drying power.

P-TSEB generated MAPD versus S-TSEB within 41·15% for DOY 174 and 8·79% for DOY 206, respectively, which indicates that P-TSEB is highly consistent with S-TSEB over low cover areas under small air drying power and less contrast in soil moisture conditions. Noticeable discrepancies occurred under large air drying power and marked contrast in soil moisture circumstances, in particular for sparse covers. Therefore, the performance of P-TSEB largely depends on meteorological and underlying surface conditions, both exerting significant influences on the coupling extent between vegetation and soil.

DOI: 10.1002/hyp

ACKNOWLEDGEMENTS

This work was jointly supported by National Natural Science Foundation of China (Grant number 40301007), the Innovation Project of the Chinese Academy of Sciences (CAS) (Kzcx2-yw-126-04) and the Innovation Project of the Institute of Geographical Sciences and Natural Resources Research, CAS (CXIOG-A05-03). This paper benefited greatly from comments of two anonymous reviewers.

REFERENCES

Allen RG, Trezza R, Tasumi M. 2006. Analytical integrated functions for daily solar radiation on slopes. *Agricultural and Forest Meteorology* **139**: 55–73.

Arnold JG, Srinivasan R, Mutttiah RS, Williams JR. 1998. Large area hydrologic modeling and assessment part I: model development. *Journal of the American Water Resources Association* **34**(1): 73–89.

Baldocchi D, Falge E, Gu L, Olson R, Hollinger D, Running S, *et al*. 2001. Fluxnet: A new tool to study the temporal and spatial variability of ecosystem-scale carbon dioxide, water vapor, and energy flux densities. *Bulletin of the American Meteorological Society* **82**(11): 2415–2434.

Batra N, Islam S, Venturini V, Bisht G, Jiang L. 2006. Estimation and comparison of evapotranspiration from MODIS and AVHRR sensors for clear sky days over the Southern Great Plains. *Remote Sensing of Environment* **103**: 1–15.

Bastiaanssen WGM. 2000. SEBAL-based sensible and latent heat fluxes in the irrigated Gediz Basin, Turkey. *Journal of Hydrology* **229**: 87–1000.

Bastiaanssen WGM, Menenti M, Feddes RA, Holtslag AAM. 1998a. A remote sensing surface energy balance algorithm for land (SEBAL): 1. Formulation. *Journal of Hydrology* **212–213**: 198–212.

Bastiaanssen WGM, Pelgrum H, Wang J, Ma Y, Moreno JF, Roerink GJ, Wal TVerDer. 1998b. A remote sensing surface energy balance algorithm for land (SEBAL): 2. Validation. *Journal of Hydrology* **212–213**: 213–229.

Becker F, Li Z-L. 1990. Temperature-independent spectral indices in thermal infrared bands. *Remote Sensing of Environment* **32**(1): 17–33.

Betts AK, Chen F, Mitchell KE, JanJic ZI. 1997. Assessment of the land surface and boundary layer models in two operational versions of the NCEP Eta Model using FIFE data. *Monthly Weather Review* **125**(11): 2896–2916.

Boegh E, Soegaard H, Thomsen A. 2002. Evaluating evapotranspiration rates and surface condition suing Landsat TM to estimate atmospheric resistance and surface resistance. *Remote Sensing of Environment* **70**: 329–343.

Brotzge JA, Kenneth CC. 2003. Examination of the surface energy budget: A comparison of eddy correlation and Bowen ration measurement systems. *Journal of Hydrometeorology* **4**(2): 160–178.

Brutsaert W. 1975. On a derivable formula for long-wave radiation from clear skies. *Water Resources Research* **11**: 742–744.

Brutsaert W. 1982. *Evaporation into the Atmosphere*. Reidel: Dordrecht.

Brutsaert W, Chen D. 1996. Diurnal variation of surface fluxes during thorough drying (or severe drought) of natural prairie. *Water Resources Research* **32**: 2013–2019.

Campbell GS, Norman JM. 1998. *An Introduction to Environmental Biophysics*. Springer: New York.

Chander G, Markham B. 2003. Revised landsat-5 TM radiometric calibration procedures and postcalibration dynamic ranges. *IEEE Transactions on Geoscience and Remote Sensing* **41**: 2674–2677.

Chen TS, Ohring G. 1984. On the relationship between clear sky planetary and surface albedos. *Journal of Atmospheric Sciences* **41**: 156–158.

Choudhury BJ, Monteith JL. 1988. A four-layer model for the heat budget of homogeneous land surfaces. *Quarterly Journal of the Royal Meteorological Society* **114**: 373–398.

Choudhury BJ, Ahmed NU, Idso SB, Reginato RJ, Daughtry CST. 1994. Relations between evaporation coefficients and vegetation indices studies by model simulations. *Remote Sensing of Environment* **50**: 1–17.

Crago R, Brutsaert W. 1996. Daytime evaporation and the self-preservation of the evaporative fraction and the Bowen ratio. *Journal of Hydrology* **178**(1–4): 241–255.

Gentine P, Entekhabi D, Chehbouni A, Boulet G, Duchemin B. 2007. Analysis of evaporative fraction diurnal behavior. *Agricultural and Forest Meteorology* **143**: 13–29.

Hipps LE, Kustas WP. 2000. Surface evaporation and its spatial variations. In *Spatial Patterns in Catchment Hydrology*, Grayson RB, Blöschl G (eds). Cambridge University Press: Cambridge.

Jiang L, Islam S. 2001. Estimation of surface evaporation map over southern Great Plains using remote sensing data. *Water Resources Research* **37**(2): 329–340.

Kimura R, Bai L, Fan J, Takayama N, Hinokidani O. 2007. Evapotranspiration estimation over the river basin of the Loess Plateau of China based on remote sensing. *Journal of Arid Environment* **68**: 53–65.

Kite GW, Droogers P. 2000. Comparing evapotranspiration estimates from satellites hydrological models and field data. *Journal of Hydrology* **229**: 3–18.

Koepke P, Kriebel KT, Dietrich B. 1985. The effect of surface reflection and of atmospheric parameters on the shortwave radiation budget. *Advances in Space Research,* **5**: 351–354.

Kustas WP, Norman JM. 1997. A two-source approach for estimating turbulent fluxes using multiple angle thermal infrared observations. *Water Resources Research* **33**(6): 1495–1508.

Kustas WP, Norman JM. 1999. Evaluation of soil and vegetation heat flux predictions using a simple two-source model with radiometric temperature for partial canopy. *Agricultural and Forest Meteorology* **94**: 13–29.

Kustas WP, Moran MS, Humes KS, Stannard DI, Pinter PJ Jr, Hipps LE, Swiatek E, Goodrich DC. 1994. Surface energy balance estimates at local and regional scales using optical remote sensing from an aircraft platform and atmospheric data collected over semiarid rangelands. *Water Resources Research* **30**(5): 1241–1259.

Moran MS, Kustas WP, Vidal A, Stannard DI, Blanford JH, Nichols WD. 1994. Use of ground-based remotely sensed data for surface energy balance evaluation of a semiarid rangeland. *Water Resources Research* **30**(5): 1339–1349.

Nash JE, Sutcliffe JV. 1970. River flow forecasting through conceptual models. *Journal of Hydrology* **10**: 282–290.

Neitsch SL, Arnold JG, Kiniry JR, Williams JR, King KW. 2002. Soil and water assessment tool, Theoretical documentation: Version 2000. TWRI TR-191. Texas Water Resources Institute, College Station, TX.

Nichols WE, Cuenca RH. 1993. Evaluation of the evaporative fraction for parameterization of the surface, energy-balance. *Water Resources Research* **29**(11): 3681–3690.

Norman JM, Kustas WP, Humes KS. 1995. A two-source approach for estimating soil and vegetation energy fluxes in observation of directional radiometric surface temperature. *Agriculture and Forest Meteorology* **77**: 263–293.

Priestley CHB, Taylor RJ. 1972. On the assessment of surface heat flux and evaporation using large-scale parameters. *Monthly Weather Review* **100**: 81–92.

Ritchie JT. 1972. Model for predicting evaporation from a row crop with incomplete cover. *Water Resource Research* **8**: 1204–1213.

Saxton KE, Rawls WJ. 2006. Soil water characteristics estimates by texture and organic matter for hydrologic solutions. *Soil Science Society of America Journal* **70**: 1569–1578.

Shuttleworth WJ, Gurney RJ. 1990. The theoretical relationship between foliage temperature and canopy resistance in sparse crops. *Quarterly Journal of the Royal Meteorological Society* **116**: 497–519.

Shuttleworth WJ, Wallace JS. 1985. Evaporation from sparse crops-an energy combination theory. *Quarterly Journal of the Royal Meteorological Society* **111**: 839–855.

Shuttleworth WJ, Gurney RJ, Hsu AY, Ormsby JP. 1989. Fife: The variation in energy partition at surface flux sites. *IAHS Publication* **186**: 67–74.

Su Z. 2002. The surface energy balance system (SEBS) for estimation of turbulent fluxes. *Hydrology and Earth System Sciences* **6**(1): 85–99.

Su H, McCabe MF, Wood EF, Su Z, Prueger JH. 2005. Modeling evapotranspiration during SMACEX02: Comparing two approaches for local and regional scale prediction. *Journal of Hydrometeorology* **6**(6): 910–922.

Tasumi M, Allen RG, Bastiaanssen WGM. 2000. The theoretical basis of SEBAL, in 'Application of the SEBAL Methodology for Estimating Consumptive Use of Water and Streamflow Depletion in the Bear River Basin of Idaho through Remote Sensing'. Idaho Department of Water Resources, University of Idaho, Department of Biological and Agriculture Engineering. Final report, pp. 46–69.

Timmermans WJ, Kustas WP, Anderson MC, French AN. 2007. An intercomparison of the Surface Energy Balance Algorithm for Land

(SEBAL) and the Two-Source Energy Balance (TSEB) modeling schemes. *Remote Sensing of Environment* **108**: 369–384.

Van de Griend AA, Owe M. 1993. On the relationship between thermal emissivity and the normalized difference vegetation index for nature surface. *International Journal of Remote Sensing,* **14**(6): 1119–1131.

Verhoef A, De Bruin HAR, Van den Hurk BJJM. 1997. Some practical notes on the parameter kB^{-1} for sparse canopies. *Journal of Applied Meteorology* **36**: 560–572.

Wang J, White K, Robinson GJ. 2000. Estimating surface net solar radiation by use of Landsat5 TM and digital elevation models. *International Journal of Remote Sensing* **21**: 31–43.

Wang K, Li Z, Cribb M. 2006. Estimation of evaporative fraction from a combination of day and night land surface temperatures and NDVI: A new method to determine the Priestley-Taylor parameter. *Remote Sensing of Environment,* **102**: 293–305.

Wegehenkel M, Jochheim H, Kersebaum KC. 2005. The application of simple methods using remote sensing data for the regional validation of a semidistributed hydrological catchment model. *Physics and Chemistry of the Earth* **30**: 575–587.

Yunusa IAM, Walker RR, Lu P. 2004. Evapotranspiration components from energy balance, sapflow and microlysimetry techniques for an irrigated vineyard in inland Australia. *Agricultural and Forest Meteorology* **127**: 93–107.

Zhan X, Kustas WP, Humes KS. 1996. An intercomparison study on models of sensible heat flux over partial canopy surfaces with remotely sensed surface temperature. *Remote Sensing of Environment* **58**: 242–256.

Zhang WC, Chen J, Ogawa K, Yamaguchi Y. 2005. An approach to estimating evapotranspiration in the Urumqi River basin, Tianshan, China, by means of remote sensing and a geographical information system technique. *Hydrological Processes* **19**: 1839–1854.

DOI: 10.1002/hyp